

Article

Maximum Deformation Ratio of Droplets of Water-Based Paint Impact on a Flat Surface

Weiwei Xu *, Jianfei Luo, Jun Qin and Yongming Zhang

State Key Laboratory of Fire Science, University of Science and Technology of China, Hefei 230026, China; luojianf@mail.ustc.edu.cn (J.L.) qinjun@ustc.edu.cn (J.Q.) zhangym@ustc.edu.cn (Y.Z.)

* Correspondence: xuweiwei2005@163.com; Tel.: +86-551-6360-6457

Received: 3 April 2017; Accepted: 8 June 2017; Published: 19 June 2017

Abstract: In this research, the maximum deformation ratio of water-based paint droplets impacting and spreading onto a flat solid surface was investigated numerically based on the Navier–Stokes equation coupled with the level set method. The effects of droplet size, impact velocity, and equilibrium contact angle are taken into account. The maximum deformation ratio increases as droplet size and impact velocity increase, and can scale as $We^{1/4}$, where We is the Weber number, for the case of the effect of the droplet size. Finally, the effect of equilibrium contact angle is investigated, and the result shows that spreading radius decreases with the increase in equilibrium contact angle, whereas the height increases. When the dimensionless time $t^* < 0.3$, there is a linear relationship between the dimensionless spreading radius and the dimensionless time to the $1/2$ power. For the case of $80^\circ \leq \theta_e \leq 120^\circ$, where θ_e is the equilibrium contact angle, the simulation result of the maximum deformation ratio follows the fitting result. The research on the maximum deformation ratio of water-based paint is useful for water-based paint applications in the automobile industry, as well as in the biomedical industry and the real estate industry. Please check all the part in the whole passage that highlighted in blue whether retains meaning before.

Keywords: droplet; impacting and spreading; simulation; the level set method; the Navier–Stokes equation; the deformation ratio

1. Introduction

The widespread application of the impact and spread of liquid droplets in such areas as agriculture, thermal spray, lab-on-a-chip, and coating [1–3], continues to receive attention. After impact onto a solid surface, there are four possible phases proposed by Rioboo et al. [4], i.e., the kinetic phase, the spreading phase, the relaxation phase, and the wetting/equilibrium phase. After some time, the droplet reaches a maximum spreading diameter. Due to the important fluid mechanics in these processes, both experiments and numerical simulations have been implemented in recent years to research droplets' dynamic behaviors after impact, which has been helpful in understanding droplet interactions with liquid and solid surfaces.

In terms of experimental research, great efforts have been made. Roisman et al. [5] experimentally and theoretically studied the impact of a single droplet onto a dry surface by implementing the inertial effect, surface tension, viscous, and wettability. Amirfazli et al. [6–8] conducted series experiments to study the dynamic behaviors of liquid droplets under different effects, e.g., the droplet size dependence on contact angles, the electric fields on contact angles, the surface tension of droplets for different materials, and the receding contact angles of droplets and the rebound time. Mao et al. [9] presented a rebound model of a droplet upon impact. Ukiwe and Kwok [10] reported that drop impact dynamics was influenced by impact energy of the droplet at impact, physical properties of the liquid droplets and solid surface tensions. Clanet et al. [11] studied the impact of liquid droplets of low viscosity on

a super-hydrophobic surface, and the experimental results presented the maximal spreading ratio scaled as $We^{1/4}$, where We is the Weber number. Based on energy balance, Park et al. [12] predicted the maximum deformation ratio at a low-impact velocity by experiment.

On the other hand, various numerical investigations have also been carried out. Bussmann et al. [13] presented a methodology to simulate the fingering and splashing of droplet impacts onto a solid surface. Merdasi et al. [14] investigated the deformation of two droplets within microfluidic T-junctions on a solid substrate by LBM (Please define). They reported that the deformation of the two droplets increases significantly with the increase in the relative velocity of the inlet flow, droplet size, and surface tension. The flow pattern in pipe flows had been simulated for drag reducing fluids using a low Reynolds number $k-\epsilon$ model by Dhotre et al. [15].

In this study, a numerical method was adopted to simulate the impact and spread of a water-based paint droplet onto a flat steel surface. The dynamics of the impact and spread were observed and used to establish guidelines for the maximum deformation ratio due to the droplet size, impact velocity, and equilibrium contact angle. The experimental results are compared with the prediction models.

2. Numerical Method

2.1. Navier–Stokes Equations

The Navier-Stokes equations for the incompressible laminar two-phase flow are implemented, and its expression is written as:

$$\rho \frac{\partial v}{\partial t} + \rho(v \cdot \nabla) = \nabla \cdot \left[-pI + \eta(\nabla v + (\nabla v)^T) \right] + f_{stf} + \rho g, \quad \nabla \cdot v = 0 \quad (1)$$

In the above equations, v , ρ , and η denote velocity, density, and dynamic viscosity, I is the 3×3 identity matrix, g is constant and gravitational acceleration, p is pressure, and f_{stf} is the surface tension force. The surface tension force only exists at an interface which separates the droplet and air.

2.2. The Level Set Method

In order to track the interface between the two phases, the level set function of φ' is introduced. The function φ' is expressed as

$$\frac{\partial \varphi'}{\partial t} + \nabla \cdot (\varphi' v) = \alpha \nabla \cdot \left(\gamma \nabla \varphi' - \varphi'(1 - \varphi') \frac{\nabla \varphi'}{|\nabla \varphi'|} \right) \quad (2)$$

where γ is the parameter controlling the interface thickness, and α is the reinitialization parameter. Both of γ and α are set parameters. In air, $\varphi' = 0$, whereas $\varphi' = 1$ in water-based paint. In the interface of the two phase flows, $\varphi' = 0.5$. The density and viscosity are controlled by

$$\rho = \rho_1 + (\rho_2 - \rho_1)\varphi' \quad (3)$$

$$\eta = \eta_1 + (\eta_2 - \eta_1)\varphi' \quad (4)$$

In the above equations, subscript 1 denotes air and 2 denotes water-based paint. The volume fractions for air and water-based paint are determined by

$$1 = frv_1 + frv_2 \quad (5)$$

In the level set method, the surface tension force f_{stf} is calculated by

$$f_{stf} = \nabla \cdot T \quad (6)$$

In the above equation, T is expressed by

$$T = \sigma \left(\hat{I} - \left(n_n n_n^T \right) \right) \delta \tag{7}$$

where \hat{I} is the identity matrix, σ is surface tension coefficient of droplet, and the interface normal n_n , and the delta function δ are calculated by

$$n_n = \frac{\nabla \phi'}{|\nabla \phi'|} \tag{8}$$

$$\delta = 6|\phi'(1 - \phi')| |\nabla \phi'| \tag{9}$$

2.3. Model Description

A scheme of the experimental unit for the water-based paint droplet impact and spread is presented in Figure 1. In Figure 1, the radius (r_w) and the height (H) of the cylindrical computational domains are 100 μm . The diameter of the droplet is 40 μm . Impact velocities in the range of 0.9–2.0 m/s are applied. The equilibrium contact angles are in the range of 40°–120°, and the equilibrium contact angle is expressed as θ_e . In the numerical simulation, the wall boundary is the wetted wall. The velocity component normal to the wall is set to zero and is determined by

$$v \cdot n_w = 0 \tag{10}$$

A frictional boundary force (f_{stf}) is added, and its expression is written by

$$f_{\text{stf}} = -\frac{\eta}{\beta} v \tag{11}$$

In the above equation, β is the slip length.

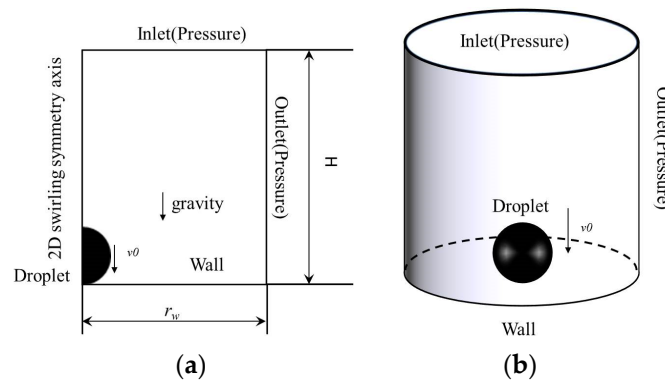


Figure 1. Schematic domain of the experiment for the water-based paint droplet impact and spread. (a) 2D; (b) 3D.

As shown in Figure 2, local mesh refinement is adopted, and the maximum mesh size is 2.9 μm in the mesh refinement region, whereas the coarse mesh is adopted in other regions. A conservative form has been used, which results in exact conservation of the mass. Some parameters for the material properties in the simulation are listed in Table 1.

In addition, several relevant numbers are defined as

$$We = \frac{\rho_2 v_0^2 D_0}{\sigma} \tag{12}$$

$$Re = \frac{\rho_2 v_0 D_0}{\eta_2} \tag{13}$$

$$\zeta_{\max} = \frac{2r_{\max}}{D_0} \quad (14)$$

$$t_d^* = \frac{t \cdot v_0}{D_0} \quad (15)$$

$$r_d^* = \frac{2r(t)}{D_0} \quad (16)$$

In the above definitions, v_0 is the initial impact velocity, r_{\max} is the maximum spreading radius of droplet, D_0 is the initial diameter of droplet, $r(t)$ is equal to half of the diameter of the droplet with variation in time, We is the Weber number, Re is the Reynolds number, ζ_{\max} is the maximum deformation ratio, t_d^* is the dimensionless time, and r_d^* is the dimensionless spreading radius. The spreading radius $r(t)$ and dynamic contact angle (θ) are defined in Figure 3.

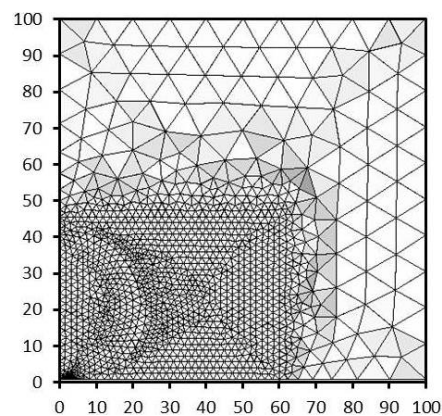


Figure 2. A typical triangular mesh of the domains.

Table 1. Material properties.

Parameter	Data
Density of the droplet(ρ_2)	1320 kg/m ³
Density of air(ρ_1)	1.225 kg/m ³
Surface tension of droplet (σ)	0.0648 N/m
Viscosity of droplet (η_2)	0.179 Pa·s
Viscosity of air(η_1)	1.7894×10^{-5} Pa·s
Gravity acceleratio (g)	$9.8 \text{ m}\cdot\text{s}^{-2}$

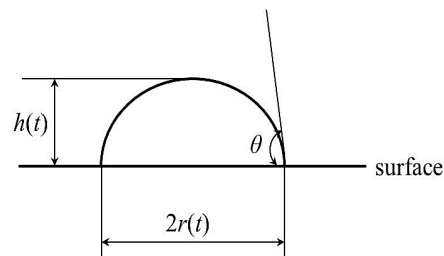


Figure 3. Sketch of a droplet of water-based paint on the solid surface after impact.

2.4. Numerical Validation

The Navier-Stokes equation has been successfully applied for the simulation of the impact and spread of liquid droplets onto solid surfaces [16,17]. To further verify the numerical validation, the simulations of the impact and spread of droplets of water-based paint onto a flat surface have been

implemented for the cases of $\theta_e = 40^\circ, 50^\circ, 80^\circ$ and 95° . Impact velocity v_0 is 1.5 m/s. The droplet diameter D_0 is 40 μm . Figure 4 presents the shape of the droplets in the final equilibrium state. The measurement software Digimizer was adopted to measure the contact angle in Figure 4, and the measurement results show that the real contact angle θ is equal to $38.4^\circ, 48.7^\circ, 82.9^\circ$ and 92.9° , respectively. Therefore, the results agree well with the theoretical solutions.

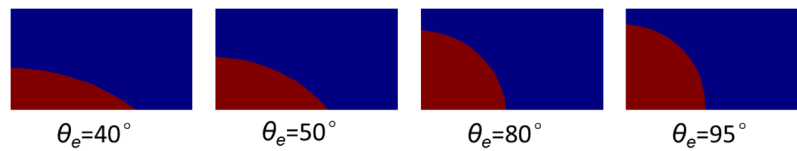


Figure 4. Shape of droplets of water-based paint with different equilibrium contact angles.

Based on the research of Vadillo et al. [18], the contact diameter is determined by

$$\frac{D_{s,e}}{D_0} \equiv 2 \left(\frac{\sin^3 \theta_e}{2(1 - \cos \theta_e)(2 - \cos \theta_e - \cos^2 \theta_e)} \right)^{1/3} \quad (17)$$

In the above equation, θ_e is the equilibrium contact angle, D_0 is 40 μm , and $D_{s,e}$ is the spreading diameter of the droplet in the equilibrium stage. Figure 5 presents the simulation results and the prediction model of Vadillo et al. θ_e is in the range of 40° – 95° in Figure 5. In Figure 5, the value of $D_{s,e}$ is equal to the final spreading diameter of the droplet for the study of the effect of the equilibrium contact angle. As shown in Figure 5, the simulation result is in accordance with the prediction model of Vadillo et al. Therefore, the Navier–Stokes equation coupled with the level set method can be used to simulate the dynamics of droplets after the impact onto the solid surface.

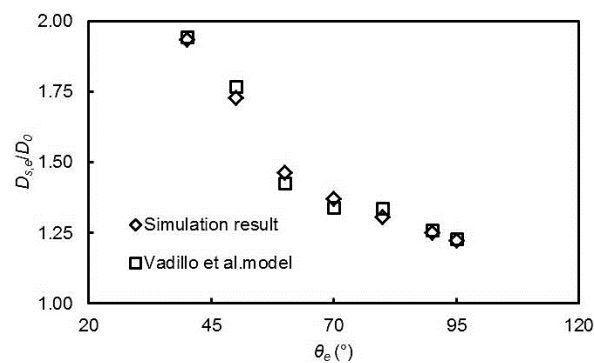


Figure 5. Comparison of the simulation result and the prediction model of Vadillo et al.

3. Results and Discussion

3.1. The Effect of Droplet Size

In this section, the effect of volume on droplet spread is investigated. Here, initial impact velocity (v_0) is 1.5 m/s, the equilibrium contact angle (θ_e) is 60° , and the initial droplet diameters (D_0) are 20, 30, 40, 50, and 60 μm . Figure 6 shows the variation in the maximum deformation ratio (ζ_{\max}) versus $We^{1/4}$ for five different volumes of water-based paint droplets. As we can see, the larger-sized droplets have greater spreading due to the greater inertia. Based on the experimental data shown in Figure 6, the ζ_{\max} associated with $We^{1/4}$ is obtained in the form of

$$\zeta_{\max} = 0.55 \cdot We^{1/4} + 0.89 \quad (18)$$

In good agreement with the experimental data, where the numerical coefficient is equal to 0.97. Therefore, we can obtain

$$\zeta_{\max} \sim We^{1/4} \quad (19)$$

The above equation agrees with the result of Clanet et al. [11].

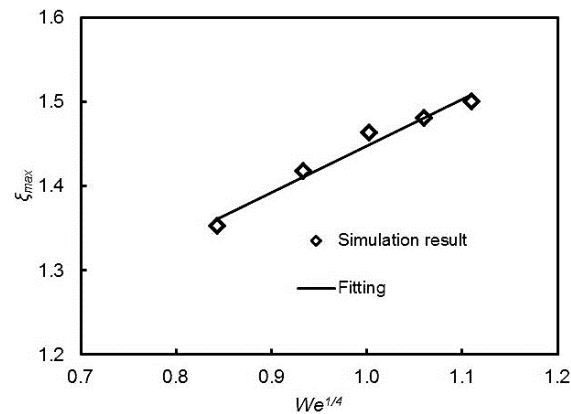


Figure 6. Maximum deformation ratio as a function of $We^{1/4}$ under different diameters.

3.2. The Effect of Impact Velocity

This section investigates the effect of impact velocity on the maximum deformation ratio of droplets. In this set of experiments, the equilibrium contact angle (θ_e) is 60° , and the initial droplet diameter (D_0) is $40 \mu\text{m}$. Figure 7 presents the results for different impact velocity of droplet. With the increase in impact velocity, ζ_{\max} increases. Based on the experimental result, we can obtain

$$\zeta_{\max} = 1.42 + 5.73 \times 10^{-2} \cdot We \quad (20)$$

In the above equation, the value of R-Square is 0.996, and a good agreement has been achieved.

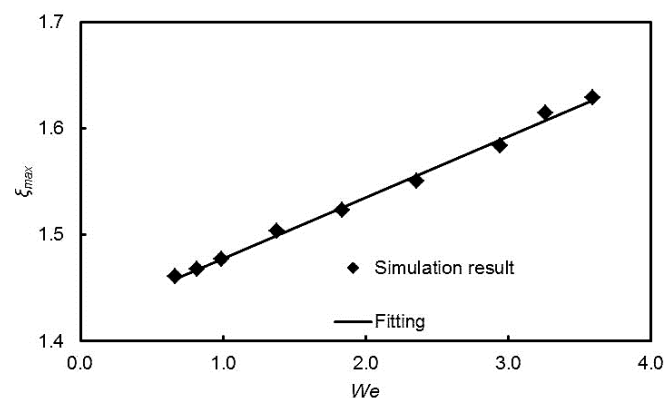


Figure 7. Maximum deformation ratio as a function of We under different impacting velocities.

According to Akao et al. [19] study, the maximum deformation ratio can be expressed as

$$\zeta_{\max} = 0.613 \cdot We^{0.39} \quad (21)$$

Senda et al. [20] proposed another prediction model on the maximum deformation ratio, and its expression is

$$\zeta_{\max} = 1 + 0.463 \cdot We^{0.345} \quad (22)$$

Figure 8 presents the experimental results and the results based on the prediction models from Akao et al. and Senda et al. In Figure 8, we can see the maximum deformation ratio increases due to the greater impact velocity, and the prediction model of Akao et al. is similar to Equation (20).

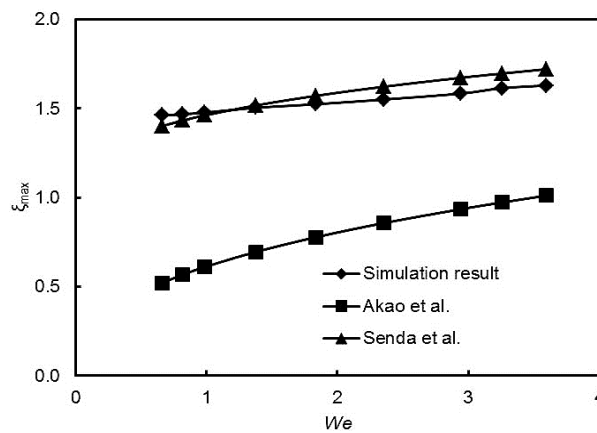


Figure 8. Comparison of the maximum deformation ratio by the experimental result and the prediction models.

3.3. The Effect of Equilibrium Contact Angle

To research the influence of the initial contact angle on the maximum deformation ratio, the initial droplet diameter (D_0) was set to 40 μm , and the initial impact velocity (v_0) to 1.5 m/s. Figure 9 shows the variation in the spreading radius ($r(t)$) and the center height ($h(t)$) with the increase in time (t) under equilibrium contact angle ($\theta_e = 40^\circ, 60^\circ$ and 120°). Figure 6 presents the variation in spreading radius and height of droplet with the time. As shown in Figure 6, the spreading radius of droplets decreases with the increase in equilibrium contact angle, whereas the height of droplet increases with the increase in equilibrium contact angle. By comparing the results for $\theta_e = 40^\circ, 60^\circ$ and 120° in Figure 9a, it has been proven that the spreading radius decreases with the increase in θ_e . For the case of $\theta_e = 40^\circ$ and 60° , the spreading radius coincides in one line, and the spreading velocity is faster than the case of $\theta_e = 120^\circ$ when time $t \leq 0.9$ ms in Figure 9a. As shown in Figure 10, the fitting curve for the case of $\theta_e = 40^\circ$ was generated to show

$$r_d^* = 0.321\sqrt{t^*} \tag{23}$$

The above equation appears to be accurate when $t^* < 0.3$. Similar expressions were obtained by Rioboo et al. [4] and Gupta et al. [21].

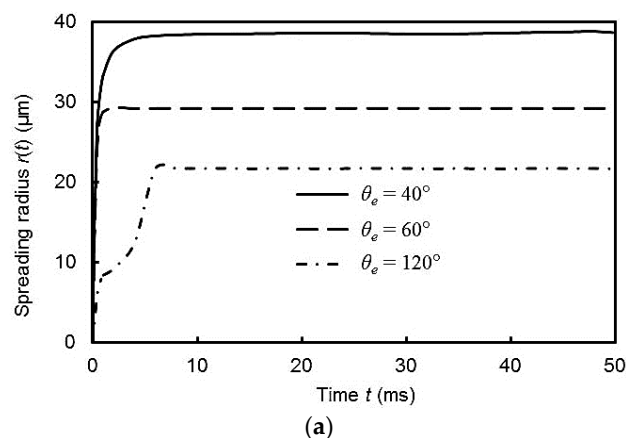


Figure 9. Cont.

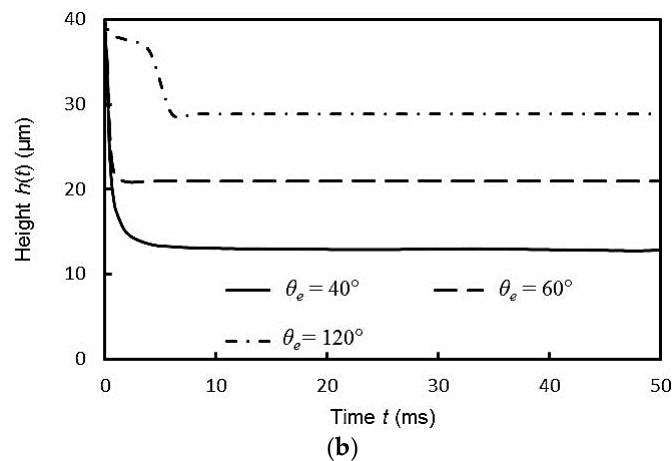


Figure 9. Variation in (a) spreading radius and (b) height versus the time.

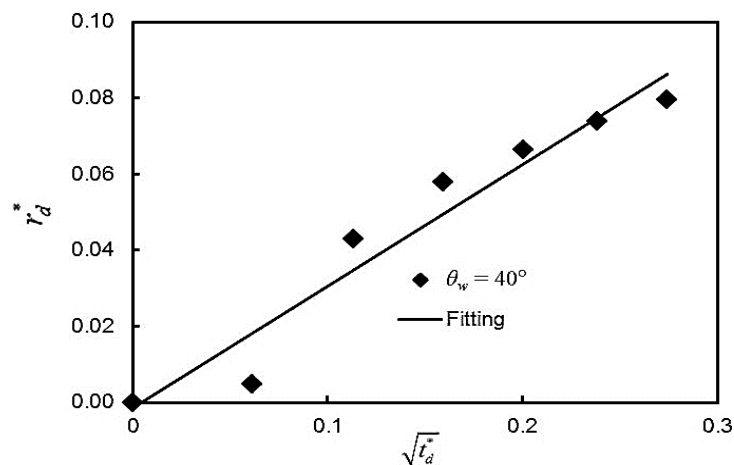


Figure 10. Variation in dimensionless spreading radius r_d^* versus $\sqrt{t_d^*}$.

Based on the research of Pasandideh-Fard et al. [22], the ζ_{\max} can be followed by

$$\zeta_{\max} = \frac{D_{\max}}{D_0} = \sqrt{\frac{We + 12}{3(1 - \cos \theta_a) + 4(We/\sqrt{Re})}} \tag{24}$$

In the above equation, θ_a is the advancing contact angle. Under different equilibrium contact angles, θ_a is different, and the actual value of θ_a in the simulation is obtained by Digimizer. Figure 11 presents the variation in ζ_{\max} versus the set equilibrium contact angle. As shown in Figure 11, ζ_{\max} decreases with the increase in equilibrium contact angle. The fitting line in Figure 11 is the best fit of the results of the prediction model obtained by Pasandideh-Fard et al. [19], and the relation between ζ_{\max} and θ_e can be described as

$$\zeta_{\max} = 2 \times 10^{-9}\theta_e^5 - 7 \times 10^{-7}\theta_e^4 + 1 \times 10^{-4}\theta_e^3 - 7.7 \times 10^{-3}\theta_e^2 + 0.267\theta_e - 2.04 \tag{25}$$

The R-Square is equal to 0.997 in the fitting. Simulation results are compared with the expression of Equation (25) as shown in Figure 11, and the results agree well with Equation (25) for $80^\circ \leq \theta_e \leq 120^\circ$.

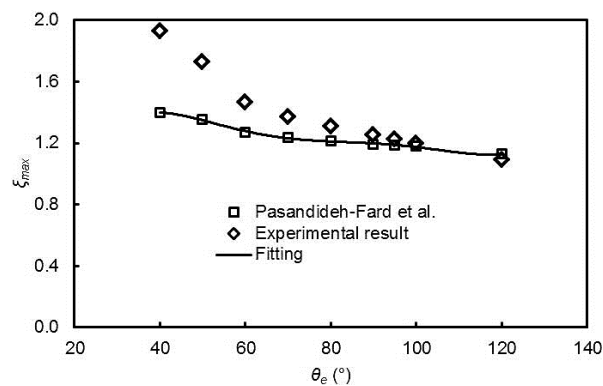


Figure 11. Variation in ζ_{max} versus θ_e .

4. Conclusions

In summary, the maximum deformation of water-based paint droplets was studied by numerical simulation based on the Navier-Stokes equations coupled with the level set method. Here, the effects of droplet size, impact velocity, and initial contact angle on the maximum deformation ratio of the water-based paint droplet were investigated. By the variation in the above three parameters, the maximum deformation ratio would change. As droplet size increased, the maximum deformation ratio of droplet scaled as $We^{1/4}$. As impact velocity increased, the maximum deformation ratio increased, and there was a linear relation between the maximum deformation ratio and We . Finally, the effect of equilibrium contact angle was studied, and the results showed a relation between the maximum deformation ratio and equilibrium contact angle.

Acknowledgments: This work was supported by the National Natural Science Foundation of China under Grant No. 41675024, the National Key Research and Development Plan under Grant No. 2016YFC0800100, and the Fundamental Research Funds for the Central Universities under Grant No. WK2320000032. The authors gratefully acknowledge all of these supports.

Author Contributions: Weiwei Xu and Jun Qin conceived and designed the experiments; Weiwei Xu performed the simulation; Weiwei Xu analyzed the data; Weiwei Xu wrote the paper, and Yongming Zhan revised the paper. Jianfei Luo contributed analysis tools.

Conflicts of Interest: The authors declare no conflict of interest.

References

- Bergeron, V.; Bonn, D.; Martin, J.Y.; Vovelle, L. Controlling droplet deposition with polymer additives. *Nature* **2000**, *405*, 772–775. [[CrossRef](#)] [[PubMed](#)]
- Fauchais, P.; Vardelle, A.; Dussoubs, B. Quo vadis thermal spraying? *J. Ther. Spray Technol.* **2001**, *1*, 44–66. [[CrossRef](#)]
- Mugele, F.; Baret, J. Electrowetting: From basics to applications. *J. Phys. Condens. Matter* **2005**, *17*, R705–R774. [[CrossRef](#)]
- Rioboo, R.; Marengo, M.; Tropea, C. Time evolution of liquid drop impact onto solid, dry surfaces. *Exp. Fluids* **2002**, *33*, 112–124. [[CrossRef](#)]
- Roisman, I.V.; Horvat, K.; Tropea, C. Spray impact: Rim transverse instability initiating fingering and splash, and description of a secondary spray. *Exp. Fluids* **2006**, *18*, 102104. [[CrossRef](#)]
- Amirfazli, A.; Kwok, D.Y.; Gaydos, J.; Neumann, A.W. Line Tension Measurements through Drop Size Dependence of Contact Angle. *J. Colloid Interface Sci.* **1998**, *205*, 1–11. [[CrossRef](#)] [[PubMed](#)]
- Bateni, A.; Laughton, S.; Tavana, H.; Susnar, S.S.; Amirfazli, A.; Neumann, A.W. Effect of electric fields on contact angle and surface tension of drops. *J. Colloid Interface Sci.* **2005**, *283*, 215–222. [[CrossRef](#)] [[PubMed](#)]
- Antonini, C.; Villa, F.; Bernagozzi, I.; Amirfazli, A.; Marengo, M. Drop rebound after impact: The role of the receding contact angle. *Langmuir* **2013**, *29*, 16045–16050. [[CrossRef](#)] [[PubMed](#)]

9. Mao, T.; Kuhn, D.C.S.; Tran, H. Spread and rebound of liquid droplets upon impact on flat surfaces. *AIChE J.* **1997**, *43*, 2169–2179. [[CrossRef](#)]
10. Ukiwe, C.; Kwok, D.Y. On the maximum spreading diameter of impacting droplets on well-prepared solid surfaces. *Langmuir* **2005**, *21*, 666–673. [[CrossRef](#)] [[PubMed](#)]
11. Clanet, C.; Béguin, C.; Richard, D.; Quéré, D. Maximal deformation of an impacting drop. *J. Fluid Mech.* **2004**, *517*, 199–208. [[CrossRef](#)]
12. Park, H.; Carr, W.W.; Zhu, J.; Morris, J.F. Single drop impact on a solid surface. *AIChE J.* **2003**, *49*, 2461–2471. [[CrossRef](#)]
13. Bussmann, M.; Chandra, S.; Mostaghimi, J. Modeling the splash of a droplet impacting on a solid surface. *Phys. Fluids* **2000**, *12*, 3121–3132. [[CrossRef](#)]
14. Merdasi, A.; Ebrahimi, S.; Moosavi, A.; Shafii, M.B.; Kowsary, F. Numerical simulation of collision between two droplets in the T-shaped microchannel with lattice Boltzmann method. *AIP Adv.* **2016**, *6*, 115307. [[CrossRef](#)]
15. Dhotre, M.T.; Ekambara, K.; Joshi, J.B. CFD simulation of the Flow Pattern for Drag Reducing Fluids in Turbulent Pipe Flows. *J. Chem. Eng. Jpn.* **2007**, *40*, 304–311. [[CrossRef](#)]
16. Roghair, I.; Musterd, M.; Ende, D.V.D.; Kleijn, C.; Kreutzer, M.; Kreutzer, M.; Mugele, F. A numerical technique to simulate display pixels based on electrowetting. *Microfluid. Nanofluid.* **2015**, *19*, 465–482. [[CrossRef](#)]
17. Ghazian, O.; Adamiak, K.; Castle, G.S.P. Spreading and retraction control of charged dielectric droplets. *Colloid Surf. A* **2014**, *448*, 23–33. [[CrossRef](#)]
18. Vadillo, D.C.; Soucemarianadin, A.; Delattre, C.; Roux, D.C.D. Dynamic contact angle effects onto the maximum drop impact spreading on solid surfaces. *Phys. Fluids* **2009**, *21*, 122002. [[CrossRef](#)]
19. Akao, A.; Araki, K.; Mori, S.; Moriyama, A. Deformation behaviors of a liquid droplet impinging on to hot metal surface. *Trans. Iron Steel Inst. Jpn.* **1980**, *20*, 737–743. [[CrossRef](#)]
20. Senda, J.; Kanda, T.; Al-Roub, M.; Farrell, P.V.; Fukami, T.; Fujimoto, H. *Modeling Spray Impingement Considering Fuel Film on the Wall*; SAE International: New York, NY, USA, 1997; Volume 970047, pp. 37–51.
21. Gupta, A.; Kumar, R. Droplet impingement and breakup on a dry surface. *Comput. Fluids* **2010**, *39*, 1696–1703. [[CrossRef](#)]
22. Pasandideh-Fard, M.; Qiao, Y.M.; Chandra, S.; Mostaghimi, R. Capillary effects during droplet impact on a solid surface. *Phys. Fluids* **1996**, *8*, 650–659. [[CrossRef](#)]



© 2017 by the authors. Licensee MDPI, Basel, Switzerland. This article is an open access article distributed under the terms and conditions of the Creative Commons Attribution (CC BY) license (<http://creativecommons.org/licenses/by/4.0/>).